

Article

Multi-Indicator Early-Warning Model for Mine Water Inrush at the Yushen Mining Area, Shaanxi Province, China

Jinxi Liang^{1,2}, Wanghua Sui^{1,*} , Ge Chen^{1,2} , Hujun Ren³ and Xibin Li³

¹ School of Resources and Geosciences, Institute of Mine Water Hazard Prevention and Control Technology, China University of Mining and Technology, Xuzhou 221116, China; liangjinxi@cumt.edu.cn (J.L.); chen_ge_cugb@163.com (G.C.)

² National Coal Mine Water Hazard Prevention Engineering Technology Research Center, Suzhou 234000, China

³ China Coal Hydrogeological Bureau Group Company, Tianjin 300131, China; lb13010027@cumt.edu.cn (H.R.); binxili88@163.com (X.L.)

* Correspondence: suiwanghua@cumt.edu.cn

Abstract: Previously conducted studies have established that the early warning of water inrush is crucial for the prevention and control of mining water catastrophes in the panel. In order to ensure the safety of coal mining, in this paper, monitoring indicators were determined using the sensitivity analysis method, and then a multi-indicator early-warning model for water inrush was established mainly based on the geological data of the Yanghuopan coal mine. The monitoring stage of the early-warning model should be determined according to the distance between the monitoring borehole and the mining position. Then, the development of a water-conducting fracture zone and the fluctuation and stochastic oscillator of monitoring indicators are comprehensively analyzed to determine the early-warning level. A multi-indicator early-warning model was applied to panel 30302 of the Yanghuopan coal mine and panel 1304 of the Zhaoxian coal mine in the Yushen mining areas. The abnormal warning of the water disaster in panel 1304 was sent 3 days before the disaster, which shows the effectiveness of the model. It can provide a reference for the development of an early-warning model for mine water inrush in Yushen mining areas.



Citation: Liang, J.; Sui, W.; Chen, G.; Ren, H.; Li, X. Multi-Indicator Early-Warning Model for Mine Water Inrush at the Yushen Mining Area, Shaanxi Province, China. *Water* **2023**, *15*, 3910. <https://doi.org/10.3390/w15223910>

Academic Editor: David Post

Received: 18 October 2023

Revised: 2 November 2023

Accepted: 7 November 2023

Published: 9 November 2023



Copyright: © 2023 by the authors. Licensee MDPI, Basel, Switzerland. This article is an open access article distributed under the terms and conditions of the Creative Commons Attribution (CC BY) license (<https://creativecommons.org/licenses/by/4.0/>).

Keywords: coal mining safety; real-time monitoring; sensitivity analysis; water-conducting fractured zone; stochastic oscillator

1. Introduction

The spatial position, combination, and interaction between the mining coal seam and aquifer, aquifuge, water pathways [1], hydrogeological barriers, and mining panels complicate the mine's hydrogeological structure, resulting in a variety of mining water disasters [2]. According to the State Administration of Work Safety in China, there were over 1000 coal mine water-inrush accidents from 2000 to 2021, resulting in over 4300 deaths. Mining water disasters are one of the most serious risks to coal mining output [3]. It is of great significance to understand the characteristics of coal mine water for the prevention and control of water inrush [4]. The amount of non-traditional energy is not enough to meet the huge and growing energy demand, which means that coal still remains the only reliable reserve in many countries for the next few decades [5]. Although the development direction of coal mining is mechanization [6] and intelligence, mine water disasters are still endless. To ensure safe production, many rules and regulations, such as the Coal Mine Safety Rules (Version 2022) and the Detailed Rules for Mine Water Prevention and Control (Version 2018), have been enacted. Mining predecessors have detailed a series of technical procedures for the prevention and control of water disasters as follows: investigation, prevention [7], blockage [8], drainage, interception, and monitoring [4], which should be integrated with mining water disaster control experience. Monitoring and early warning play an important

role among these factors [9]. The precursor of water inrush is characterized by some main stress–strain parameters, geophysical parameters, and hydrogeological parameters [10,11]. It is often accompanied by informational changes in the mining environment, such as seepage, displacement, stress, and temperature field [12]. Water pressure, temperature [13], rock stress, and strain, as well as hydrochemical [14] and microseismic indicators, are all monitoring indicators of the early-warning system [15], which can be used for the early warning of water inrush in mines [16]. Water sources and pathways are the main monitoring aspects for the early warning of the mine water inrush [17]. With the mining of the panel, the pressure and temperature of groundwater change due to the connection of aquifers on different horizons [9]. At the end of the last century, a monitoring system of water inrush from the seam floor was established [18] for the first time, with four sensors for temperature, water pressure, stress, and strain. It predicted a floor water inrush accident successfully. Water disasters can be predicted by identifying the charge of ions in mining water because there are differences in the composition and concentration of ions in different water sources [19,20]. Moreover, rock bursts often produce hydraulic pathways, even inducing a water inrush disaster [21]. Through microseismic monitoring, the focal mechanism solution of the anomalous area is reversed to realize an early warning of water inrush [22]. Researchers are also put forward to detect the burst signal as an early-warning sign of mine disasters [23]. Other researchers combine multi-source information technology for early warnings, such as a normal cloud model to dynamically assess mine water inrush risk [24]. A convolutional neural network [25], fuzzy mathematics [26], analytic hierarchy processing [27], and other analytical methods have been applied to quickly identify water inrush sources. Of course, precursor warning is not limited to water inrush. For example, the behavior of the surrounding rock mass can be predicted by watching the set value of the roof sagging continuously in time [28]. Wireless sensors are used to identify explosives in the air and monitor their concentration so as to analyze the risk of mining explosions [29].

Because of the complexities and the relationship among aquifer types, aquifer characteristics, flow patterns, and mining excavation, it is difficult to predict the inflow of mine water [30]. The goal of early warning is to infer and anticipate mining water hazards using immediate and direct parameters rather than indirect ones, i.e., to predict water disasters using basic measurable factors [31]. However, the threshold-setting techniques in existing early-warning models are subjective, leading to the inaccurate identification of a water inrush. During mining, the threshold value fluctuates depending on the monitoring scenario. Through the monitoring and real-time analysis of each indicator during mining, the program obtains the judgment result of the mine water inrush in time. Corresponding software can be developed to reduce the operation difficulties of field staff. The purpose of this study is to create a real-time early-warning model based on sensitivity analysis to choose the relevant indicators according to the mine's hydrogeological structure. Other mines can refer to this model and formulate specific suitable indicators and early-warning thresholds according to their own conditions.

2. Methods Section

2.1. Field Monitoring

The parallel network electricity method with an arrangement of Wenner α (Figure 1) was adopted in this study for the collection of apparent resistivity. A unipolar power supply was used (Equations (1) and (2)).

$$\rho_s^\alpha = k^\alpha \frac{\Delta U^\alpha}{I} \quad (1)$$

$$k^\alpha = 2\pi a \quad (2)$$

where ρ_s is apparent resistivity; ΔU is the voltage; a is the spacing of the electrode ($a = AM = MN = NB$).

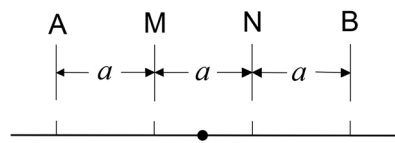


Figure 1. Schematic diagram of Wenner α .

Brillouin optical time domain reflectometer (BOTDR) is used for optical fiber monitoring. Equation (3) gives the relationship between the strain on the optical fiber and the axial Brillouin frequency drift [32].

$$v_B(\varepsilon) = v_B(0) + \frac{d_{v_B}(\varepsilon)}{d_\varepsilon} \varepsilon \tag{3}$$

where $v_B(\varepsilon)$ is the Brillouin frequency drift when the fiber is subjected to strain ε ; $v_B(0)$ is the Brillouin frequency drift when the optical fiber is free in the test environment; $\frac{d_{v_B}(\varepsilon)}{d_\varepsilon}$ is the strain coefficient; and ε is the axial strain of optical fiber.

2.2. Sensitivity Analysis

One of the strategies widely used to examine uncertainty is sensitivity analysis. The influence degree of different factors on the output results can be derived by evaluating the regular pattern and the influence of factors on the output results, and then the capacity of a project to tolerate risks can be judged [33]. If a slight change in a parameter causes a substantial change in an index, that parameter is a sensitive factor of the index; otherwise, it is a non-sensitive factor on the index. The sensitive factors of water inrush can be successfully identified via sensitivity analysis. Varying panels in various coal mines have different effect indices [34]. Indices should be determined according to the geological and hydrogeological conditions of the study area. The sensitivity indicators chosen for this water inrush early-warning model differed slightly from traditional sensitivity factors, which are appropriate for diverse conditions. The traditional sensitivity analysis highlights the impact of variables on the output outcomes [35]. Water inrush is affected by factors such as the thickness of the mining coal seam and the availability of water in the aquifer. Under the same conditions, the higher the thickness of the coal seam, the greater the likelihood of water inrush. The water inrush-sensitive indicators considered at this time were those sensitive to water inrush but which could not anticipate or affect its occurrence. When water inrush occurred, however, these signs were easier to observe, and their response (change) was faster.

$$d_i(X) = \frac{y(x_1, \dots, x_{i-1}, x_i + \Delta, x_{i+1}, \dots, x_k) - y(X)}{\Delta} \tag{4}$$

The elementary effect of the i -th parameter is described as Equation (4) for a given $X = (x_1, x_2, \dots, x_k)$, where d is a value in $1/(p - 1), \dots, 1 - 1/(p - 1)$ and p is the number of levels [36].

In the actual mining process, indicators should be chosen based on various hydrogeological conditions. Concerning the risk of water inrush, F is regarded as a function of each factor x_i (Equation (5)). The sensitivity degree (Equation (6)) can be obtained by analyzing the sensitivity of each parameter to determine the grading mode.

$$F = f(X_1, X_2, X_3, \dots, X_n) \tag{5}$$

$$S_i = \frac{\left[\frac{\Delta F_i}{F_i} \right]}{\left[\frac{\Delta X_i}{X_i} \right]} \tag{6}$$

The determination of monitoring indicators via sensitivity analysis is a relatively complicated process. First, it is important that whenever we obtain information about a mining area, we also receive a lot of information on engineering geology and hydrogeology, such as strata, rock and soil strength, water level, water inflow, and so on. Some of these parameters can be used to evaluate or predict the danger of water inrush in this mining area, such as formation strength, mining depth, coal thickness, and so on, but they are not suitable for early warning. There are still some parameters that cannot determine whether water inrush occurs or not, but carry disaster precursor information, so we can realize disasters and receive an early warning through these ‘sensitive’ parameters.

There are two ways to screen monitoring indicators via the sensitivity analysis method. The first way (Equations (5) and (6)) is to analyze the variation range in each parameter when a water inrush disaster occurs in similar mining areas. For example, a water inrush accident occurred in the Taoyuan coal mine in 2014, and the Ordovician limestone water level dropped by about 2 m within 5 h [20]. In addition, in the Zhaoxian coal mine studied in this paper, before the disaster, the water level went down continuously, which triggered the threshold and issued an early warning. By analyzing the sensitivity of precursor information contained in different parameters to disasters, we can determine monitoring indicators. We should also note that different precursor indicators show different changes in the same disaster. For example, if the water level drops by only a few meters, a change of 0.5 °C in water temperature can reflect a major flood accident while the water inflow needs to be doubled [20]. Therefore, we put forward two modes, the variable value and variable amplitude, to evaluate the monitoring indicators, respectively. The second method uses the Sobol sensitivity analysis method. Its basic principle is based on Equation (4). We need to determine the monitoring indicators by evaluating the Sobol indices of each parameter through the mathematical model of mine water disaster prediction. If the mathematical model is not perfect, the monitoring index can also be determined using sensitivity analysis combined with machine learning. This paper mainly determines the monitoring index via the first method.

2.3. Stochastic Oscillator

The stochastic oscillator, invented by George C. Lane in the late 1950s, is a momentum indicator that indicates the closing value in relation to its value range over time. This method was originally employed for future market analysis [37], and it is now frequently utilized for stock market short- and medium-term trend research [38]. The stochastic oscillator is formed from the statistical theory of integrating the notions of momentum, the strength index, and moving average while calculating the Row Stochastic Value (RSV) through the maximum, minimum, and final value of a period. This method aims to predict the turning point of the monitoring index by comparing the current value of the monitoring index with its fluctuation interval [39]. Because stochastic is simply a concept of random fluctuation, the trends of the K , D , and J lines can be used to make short-term and medium-term forecasts. The stock and futures markets also follow natural laws, meaning that it is possible to predict the price trend of the market using mathematical techniques rather than relying on random fluctuations. We can determine when the stock price will be adjusted back and what price it will be adjusted back to using these trading orders [40]. The main body of the stock market is humans, while the main body of mining disasters is nature. Humans are frequently more complex than nature. Humans utilize data to mislead their opponents, and the information released by natural disasters is always accurate. We strove to combine this method with the early-warning model, according to its principles, to obtain a more accurate early warning of mine water inrush.

$$RSV = \frac{C - L_n}{H_n - L_n} \times 100 \quad (7)$$

$$K_i = (2K_{i-1} + RSV_i) / 3 \quad (8)$$

$$D_i = (2D_{i-1} + K_i) / 3 \tag{9}$$

$$J_i = 3K_i - 2D_i \tag{10}$$

where C is the value at the end of a monitoring period, L_n is the minimum value in n days, H_n is the maximum value in n days, K_i , D_i , and RSV_i , respectively, represent the K value, D value, and RSV value of the day, K_{i-1} represents the K value of the previous day, and if there is no K value in the previous day, it is replaced by 50 as well as D_{i-1} .

2.4. Development of the Early-Warning Model

The monitoring process of precursor indicators is the monitoring procedure of the early warning model. In conjunction with the geological background of the research region and the current monitoring tools, the following five monitoring indicators were chosen for the early warning of mine water inrush: microstrain, apparent resistivity, water level, mine water inflow, and water temperature.

The model was separated into two stages based on whether or not the panel reached the effective monitoring distance, which was determined to be 50 m. The first stage occurred when the panel was not mined to the effective monitoring distance, which is primarily determined by the optical fiber, and the parallel network electricity method was used to monitor and judge the location of the water-conducting fractured zone and the water-rich abnormal area. Stage 2 comprises two sub-models when the panel was mined to the effective monitoring distance: the real-time identification of water-conducting fractured zones and real-time monitoring of sensitive indicators. Figure 2 shows the flow chart of an early-warning system.

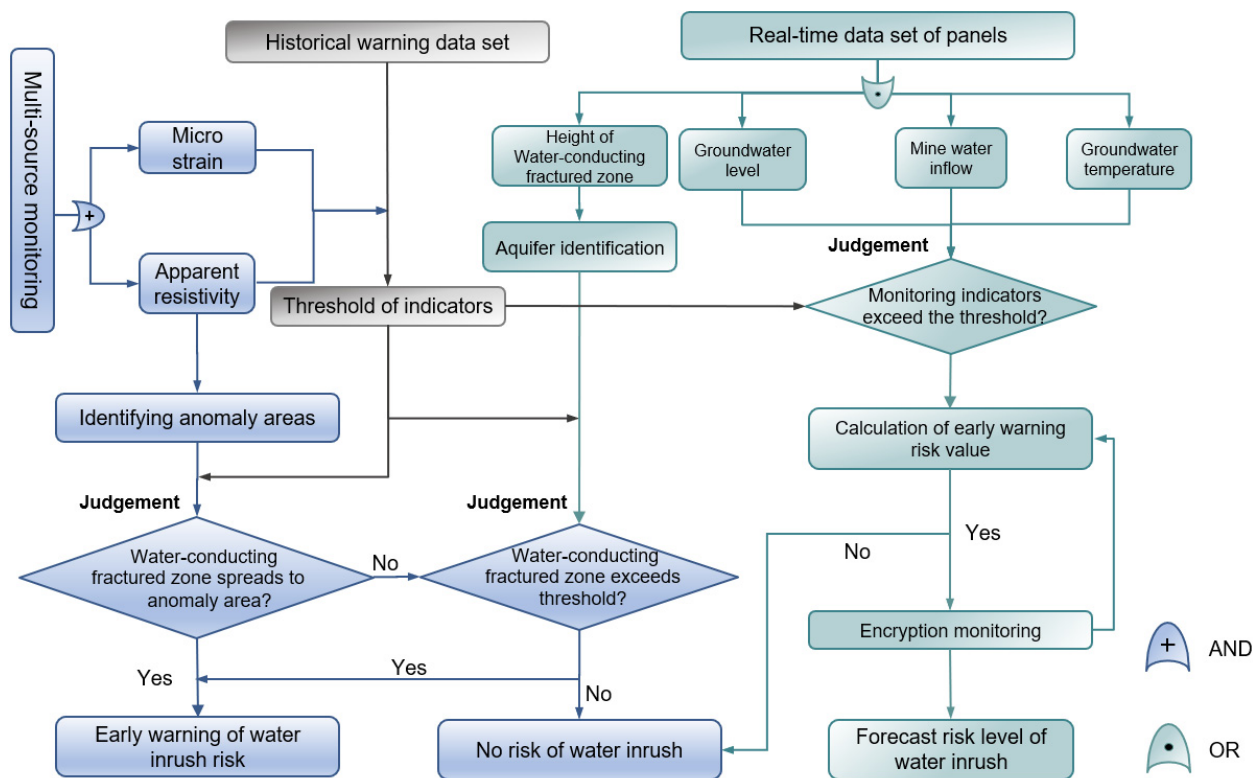


Figure 2. Flow chart of an early-warning model.

Five indicators, including the strain of optical fiber, apparent resistivity, groundwater level, mine water inflow, and mine water temperature, were selected.

The median absolute deviation (MAD) was adopted to evaluate the strain of optical fiber (Equation (11)). MAD is a measure of statistical dispersion and a robust statistic, which is more suitable for outliers in the data set than the standard deviation. Five, seven, ten, fifteen, and twenty times were used as the boundaries of the abnormal, low, medium, high, and extremely high-risk warnings.

$$\text{MAD} = 1.4826(\text{median}(|\varepsilon_i - \text{median}(\varepsilon)|)) \quad (11)$$

where ε_i is the real-time monitoring value of the microstrain.

In the event of a mining water inrush, the increase in mine water inflow could exceed more than 23 times the warning reference value. The variable amplitude mode was adopted to evaluate the anomaly of mine water inflow and apparent resistivity in this work.

Normally, the variation in water temperature does not exceed 0.5 °C within 15 days [20], but it clearly changes during water inrush. The variable value mode is adopted to warn the indicator of water temperature, as well as the groundwater level. In the typical case of water inrush in the coal mine adjacent to the study area, the groundwater level does not drop more than 20 m within six hours after the occurrence of water disasters [41].

The essence of a grading warning is to calibrate the normal interval of indicators and the threshold based on monitoring data. Variable value and variable amplitude modes are proposed based on each monitoring indicator's sensitivity to water inrush. Using water temperature and inflow as an example, the monthly average water temperature in the study area changes and does not exceed 1 °C according to monitoring data. If the water temperature varies by 0.5 °C in a short period of time (within 24 h), there is a high likelihood of water inrush. The water inflow tends to multiply before the water inrushes into the mine. For example, during the water inrush disaster at panel N1201 in the Ningtiaota coal mine, the water inflow increased from 45 to 179 m³/h, and water inflow increased from 50 to 200 m³/h during the water inrush disaster at the Ciyaowan coal mine. That is, the water inflow was less responsive to mine water inrush than the water temperature.

The factors that caused the mine water inrush were complicated; their dimensions were different, and some of them were qualitative, while others were quantitative [42]. Hazard sources are graded and produce an early warning by analyzing the fluctuation of data. For the convenience of defining the severity of disasters, the signal of warning is divided into five levels, namely anomaly warning, low-risk warning, medium-risk warning, high-risk warning, and extremely high-risk warning.

2.4.1. Multi-Source Monitoring

The height of the caving and fractured zone of the overburden and the rock resistivity of the water-rich rock and soil layer can be obtained according to the mining situation of the previous panels. According to the on-site monitoring data from optical fiber and electrical methods, combined with the previous water-rich situation of rock and soil layers, the geophysical anomaly area can be identified. A geophysical anomaly area refers to an area that is inconsistent with the previous water-rich situation of the rock and soil layers. The empirical value must be used to determine whether the water-conducting fractured zone connects with the geophysical anomaly area, and if so, an early warning of the water inrush risk should be issued. Figure 3 shows the flow chart of the multi-source monitoring model. In addition, the on-site monitoring results show that when the mining position of the panel was more than 50 m away from the monitoring borehole, the monitoring data were not affected. Therefore, monitoring boreholes here should be laid more than 50 m away from the mining position to ensure the effectiveness of early warning.

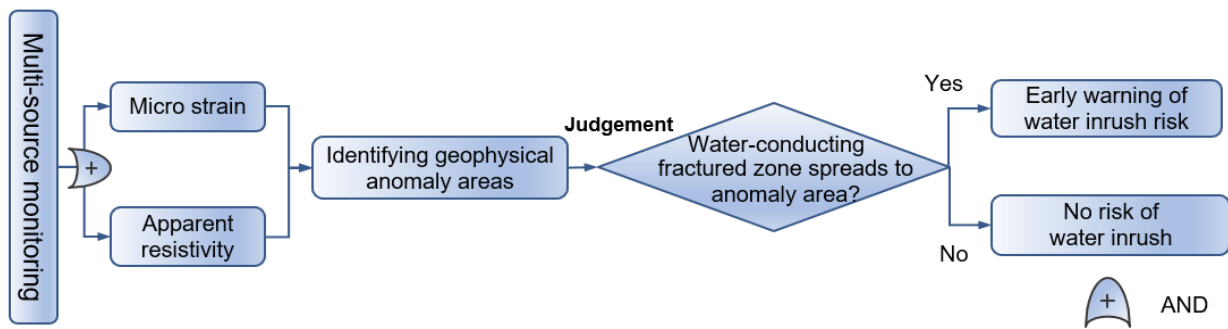


Figure 3. Flow chart of the multi-source monitoring model.

2.4.2. Real-Time Early-Warning Model

a. Model for real-time identification of the water-conducting fractured zone

The coupling analysis of the optical fiber and parallel network electricity method findings can provide a real-time judgment of the growth of the water-conducting fractured zone. If the height of the water-conducting fracture zone exceeds the threshold (the height of historical experience), the water inrush risk alert is given directly without dividing the warning level. Figure 4a shows the flow chart.

b. Model for real-time monitoring of water-sensitive indicators

On-site monitoring indicators are determined using the actual hydrogeological conditions of coal mines. During mining, a number of variables, such as the water level, pressure, and inflow, are monitored in real-time. Risk levels are computed based on their fluctuation, providing an early warning. Figure 4b depicts the flow chart.

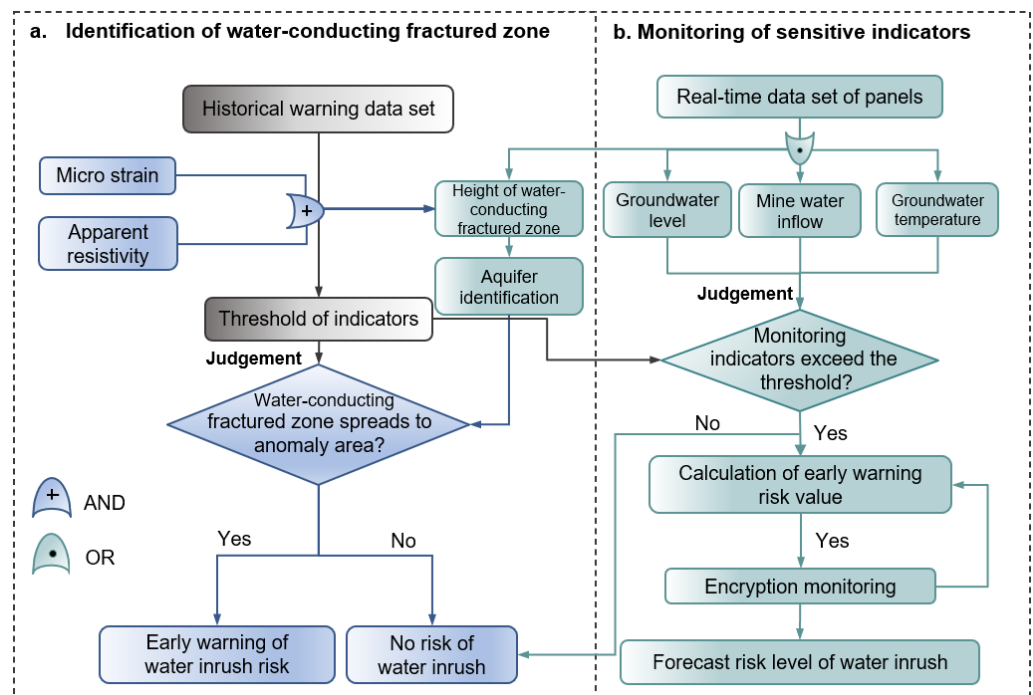


Figure 4. Flow chart of the real-time early-warning model.

2.5. Development of Multi-Indicators Early-Warning Model

Based on the characteristics of the variable value and variable amplitude, the weight of each factor is determined by the analytic hierarchy process [43]. The evaluation matrix of the variable value mode is taken as an example to describe the process of development. The results are shown in Tables 1 and 2.

Table 1. Results of AHP for variable value.

Factor	Eigenvector	Weight	Characteristic Value	CI
Statistical values	0.8736	0.2493		
Short-time variable value	2.0801	0.5936	3.0536	0.0268
Long-time variable value	0.5503	0.1571		

Table 2. Results of AHP for variable amplitude.

Factor	Eigenvector	Weight	Characteristic Value	CI
Statistical values	0.7937	0.2535		
Short-time variable amplitude	1.4938	0.4771	3.0037	0.0018
Long-time variable amplitude	0.8434	0.2694		

The risk value RK (Equations (12)–(14)) is offered to quantify multi-indicator risk levels.

The multi-indicator early-warning model is divided into five levels to distinguish it from the single-factor early-warning model as follows: white, blue, yellow, orange, and red warning. This corresponds to an abnormal warning, low risk, medium risk, high risk, and extremely high risk, respectively (Table 3). Table 4 summarizes the real-time early-warning model of sensitive indicators.

$$RK = \sum f_i(x) \tag{12}$$

$$\begin{cases} f_\epsilon(x) = Sta(x) \\ f_{ps}(x) = Va_s(x) \\ f_t(x) = 0.2493Sta(x) + 0.5936Va_s(x) + 0.1571Va_l(x) \\ f_Q(x) = 0.2535Sta(x) + 0.4771Ra_s(x) + 0.2694Ra_l(x) \\ f_Z(x) = 0.2493Sta(x) + 0.5936Va_s(x) + 0.1571Va_l(x) \end{cases} \tag{13}$$

$$Level(RK) = \begin{cases} \text{White warning,} & 0 < RK < 3 \\ \text{Blue warning,} & 3 \leq RK < 8 \\ \text{Yellow warning,} & 8 \leq RK < 13 \\ \text{Orange warning,} & 13 \leq RK < 18 \\ \text{Red warning,} & RK \geq 18 \end{cases} \tag{14}$$

where RK is the risk value of monitoring indicators, $Va(lue)$ refers to the variable value mode, Va_s is a short-time value-changing mode, Va_l is a long-time value-changing warning, $Ra(nge)$ refers to amplitude warning, in which Ra_s is the short-term amplitude-changing warning, Ra_l is the long-term amplitude-changing warning, and level (RK) is the final risk level.

Table 3. Classification of multi-indicators model.

Risk Level	Riskless	White	Blue	Yellow	Orange	Red
Classification	$RK = 0$	$0 < RK < 3$	$3 \leq RK < 8$	$8 \leq RK < 13$	$13 \leq RK < 18$	$RK \geq 18$
$RK = \sum f_i(x)$	all indicators do not show any abnormal	<1/2 monitoring indexes abnormal	>1/2 monitoring indicators abnormal	>1/2 monitoring indicators low-risk	>1/2 monitoring indicators medium-risk	1/2 monitoring indicators high-risk or above
Countermeasure		Monitor intensively	Investigate the cause of abnormality	Stop working immediately	Ask water prevention experts for analysis.	

Table 4. Real-time early-warning model of sensitive indicators.

Grading of Single Indicator			Riskless	Abnormal Warning	Low-Risk Warning	Medium-Risk Warning	High-Risk Warning	Extremely High-Risk Warning
Monitoring indicators	Warning parameters	Calculation	0	1	2	3	4	5
Fiber strain ϵ	MAD	$1.4826 \times (\text{median}(\epsilon_i - \text{median}(\epsilon)))$	$\epsilon I \leq 5\text{MAD}$	$5\text{MAD} < \epsilon I \leq 7\text{MAD}$	$7\text{MAD} < \epsilon I \leq 10\text{MAD}$	$10\text{MAD} < \epsilon I \leq 15\text{MAD}$	$15\text{MAD} < \epsilon I \leq 20\text{MAD}$	$\epsilon I > 20\text{MAD}$
Apparent resistivity ($\Omega \cdot \text{m}$)	Short-time variable amplitude	$ \rho_s - \bar{\rho}_s / \rho_s$	$\rho s I(n) \leq 1$	$1 < \rho s I(n) \leq 2$	$2 < \rho s I(n) \leq 3$	$3 < \rho s I(n) \leq 4$	$4 < \rho s I(n) \leq 5$	$\rho s I(n) > 5$
Groundwater temperature ($^{\circ}\text{C}$)	Statistical	$ T - (\mu_t + 2\sigma_t) $	Within the confidence interval	$0.1 < \text{TI} \leq 0.2$	$0.2 < \text{TI} \leq 0.3$	$0.3 < \text{TI} \leq 0.5$	$0.5 < \text{TI} \leq 1$	$\text{TI} > 1$
	Short-time variable value	$ T - \bar{T}_s $	$0 < \text{TI} \leq 0.1$	$0.1 < \text{TI} \leq 0.2$	$0.2 < \text{TI} \leq 0.3$	$0.3 < \text{TI} \leq 0.5$	$0.5 < \text{TI} \leq 1$	$\text{TI} > 1$
	Long-time variable	$ T - \bar{T}_l $	$0 < \text{TI} \leq 0.1$	$0.1 < \text{TI} \leq 0.2$	$0.2 < \text{TI} \leq 0.3$	$0.3 < \text{TI} \leq 0.5$	$0.5 < \text{TI} \leq 1$	$\text{TI} > 1$
Mine water inflow (m^3/h)	Statistical	$ Q - (\mu_q + 2\sigma_q) $	Within the confidence interval	$0 < \text{QI} \leq 1$	$1 < \text{QI} \leq 2$	$2 < \text{QI} \leq 3$	$3 < \text{QI} \leq 4$	$\text{QI} > 4$
	Short-time variable amplitude	$ Q - \bar{Q}_s / \bar{Q}_s$	$0 < \text{QI}(n) \leq 0.5$	$0.5 < \text{QI}(n) \leq 1$	$1 < \text{QI}(n) \leq 2$	$2 < \text{QI}(n) \leq 3$	$3 < \text{QI}(n) \leq 4$	$\text{QI}(n) > 4$
	Long-time variable amplitude	$ Q - \bar{Q}_l / \bar{Q}_l$	$0 < \text{QI}(n) \leq 0.5$	$0.5 < \text{QI}(n) \leq 1$	$1 < \text{QI}(n) \leq 2$	$2 < \text{QI}(n) \leq 3$	$3 < \text{QI}(n) \leq 4$	$\text{QI}(n) > 4$
Water level (m)	Statistical	$ Z - (\mu_z + 2\sigma_z) $	Within the confidence interval	$0 < \text{ZI} \leq 1$	$1 < \text{ZI} \leq 2$	$2 < \text{ZI} \leq 5$	$5 < \text{ZI} \leq 10$	$\text{ZI} > 10$
	Short-time variable value	$ Z - \bar{Z}_s $	$0 < \text{ZI} \leq 0.5$	$0.5 < \text{ZI} \leq 1$	$1 < \text{ZI} \leq 2$	$2 < \text{ZI} \leq 5$	$5 < \text{ZI} \leq 10$	$\text{ZI} > 10$
	Long-time variable value	$ Z - Z_l $	$0 < \text{ZI} \leq 0.5$	$0.5 < \text{ZI} \leq 1$	$1 < \text{ZI} \leq 2$	$2 < \text{ZI} \leq 5$	$5 < \text{ZI} \leq 10$	$\text{ZI} > 10$

3. Hydrogeological and Geological Engineering Conditions

3.1. The Yanghuopan Coal Mine

The Yanghuopan coal mine is located in Shenmu City, Yulin City, Shaanxi Province, in the northern part of the loess plateau (Figure 5). The geomorphic unit belongs to the loess hilly and gully region. The research area's topography has an elevation range of 1100–1250 m and a relative height difference of 150 m, with a tendency to be higher in the northeast and lower in the southwest. Figure 1 shows the study field, which covers an area of approximately 378,390 m².

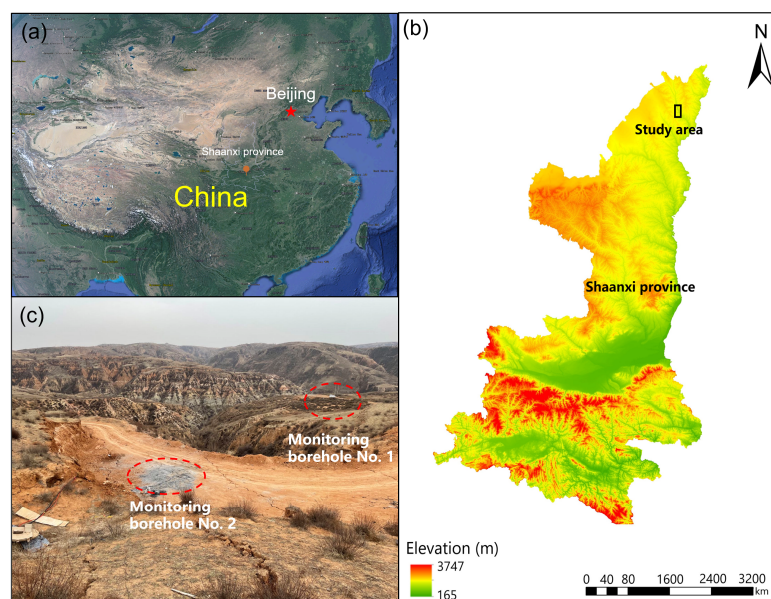


Figure 5. Location of the study area and field photo. (a) Shaanxi province. (b) Study area. (c) field photo.

Two monitoring boreholes were set up at the study panel. The boreholes contained electrodes and optical fibers. An 80 m long optical fiber and 48 electrodes spaced 2.2 m each apart were installed in monitoring borehole No. 1. The optical fiber measured 95 m in length in monitoring borehole No. 2, and 54 electrodes were spaced 1.8 m apart. From 26 February 2022 to 7 April 2022, there was a 51-day field monitoring period. A total of 115 sets of stress–strain data and 37 sets of apparent resistivity data were gathered.

3.2. Lithology and Hydrogeology

The strata in the study area consist of the Quaternary, Neogene, Jurassic, and Triassic, respectively. Among them, the coal-bearing stratum is the Jurassic Yan'an Formation. The thickness of overburden of seam No. 3 ranges from 16.51 to 91.26 m. Furthermore, the thickness of Jurassic coal seam No. 3 is 1.94 m, with a dip angle between 0° and 2°. Figure 6 shows the stratigraphy of monitoring boreholes, and Figure 7 shows the geological profile of the panel.

Roof sandstone fissure water is the primary water source in the research region, with a worn bedrock thickness of 11.05 m, a water input of 0.014 L/s, salinity of 0.616 g/L, annual average precipitation of 434.4 mm (1957–2015), and yearly precipitation of 108.6 mm in the dry season (1965). The yearly precipitation in the dry season is 108.6 mm (1965), while it is 819.0 mm in the rainy season (1967). The yearly precipitation distribution is quite unequal, with rainstorms accounting for approximately 68 percent of the annual precipitation, and the precipitation differs dramatically between years.

Groundwater in roof sandstone, burnt rocks, and goaf are commonly encountered in the Ordos and surrounding coal mining areas. The local area of panel 30302 is covered with water-rich rock strata and the water-accumulated goaf of seam No. 2. Water inrush is a

problem that jeopardizes the safety production of the mine. Based on the means of existing monitoring in the study area, combined with optical fiber, the parallel network electrical method, etc., are synthetically executed to realize the early warning of water inrush.

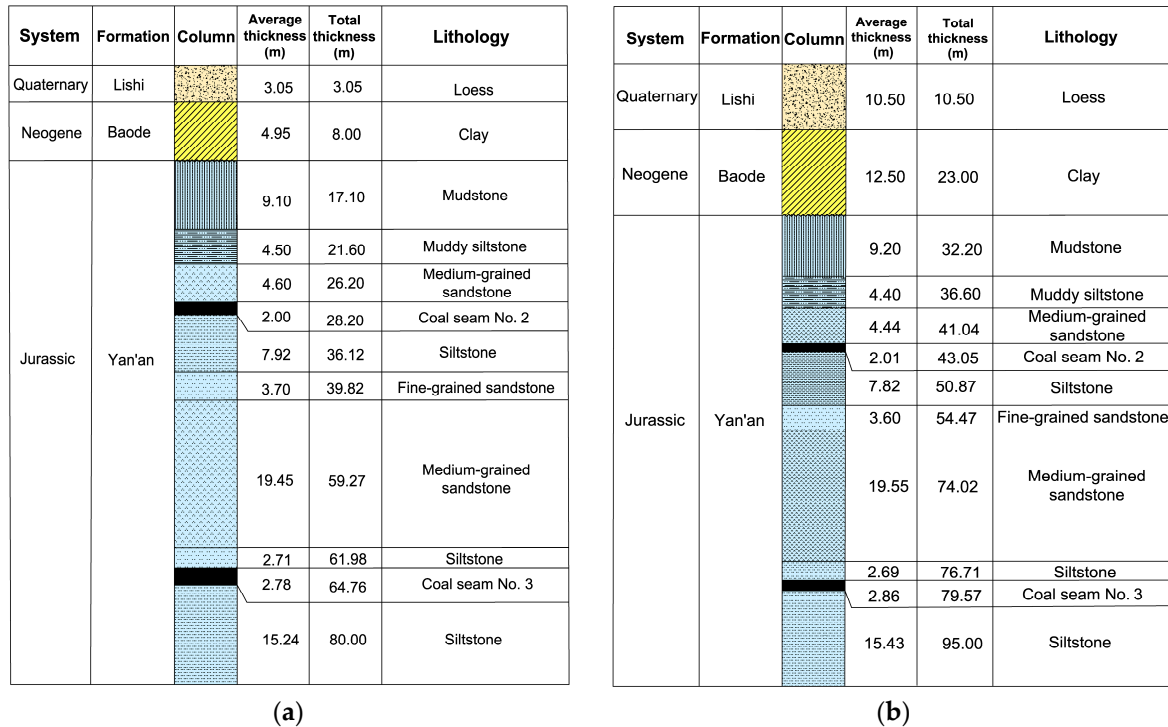


Figure 6. Stratigraphy in the Yanghuopan coal mine (a) Borehole No. 1. (b) Borehole No. 2.

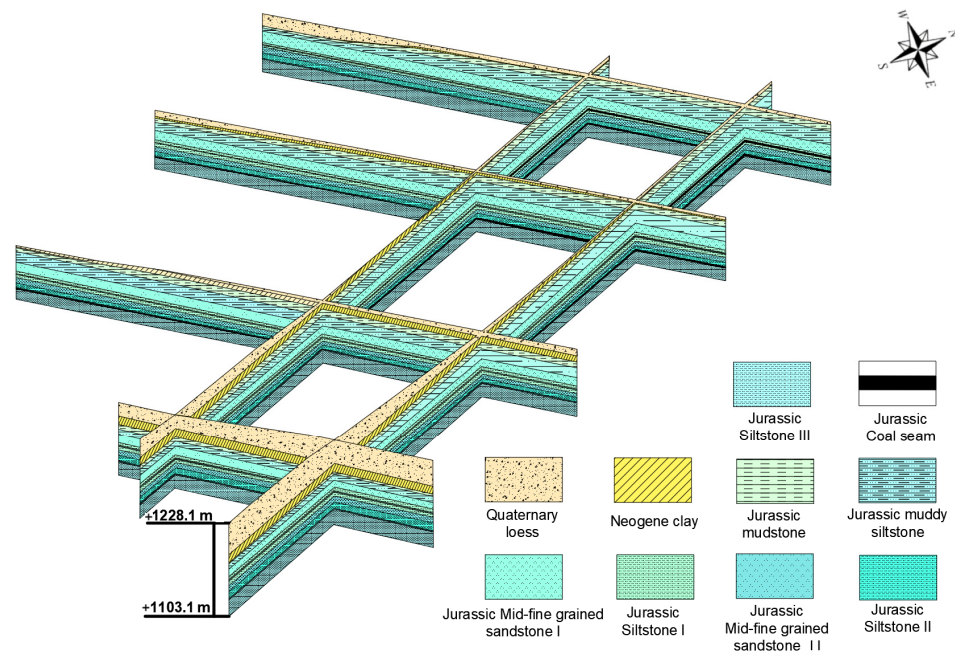


Figure 7. Geological profile of panel 30302 in the Yanghuopan coal mine.

4. Results

The numerical simulation discrete element method (DEM) is a numerical analysis method first put forward by PA Cundall and applied to the stability analysis for rock and soil masses. The three-dimensional distinct element program adopts the discrete

element method from discontinuous mechanics theory to solve discontinuous problems in geotechnical engineering.

The length, width, and height of the model are 400 m, 600 m, and 150 m, respectively (Figure 8). The damage in the material is simulated by the Mohr–Coulomb criterion, and the mined area is simulated by the excavate element. The model includes 232 block units and 308,195 zone units.

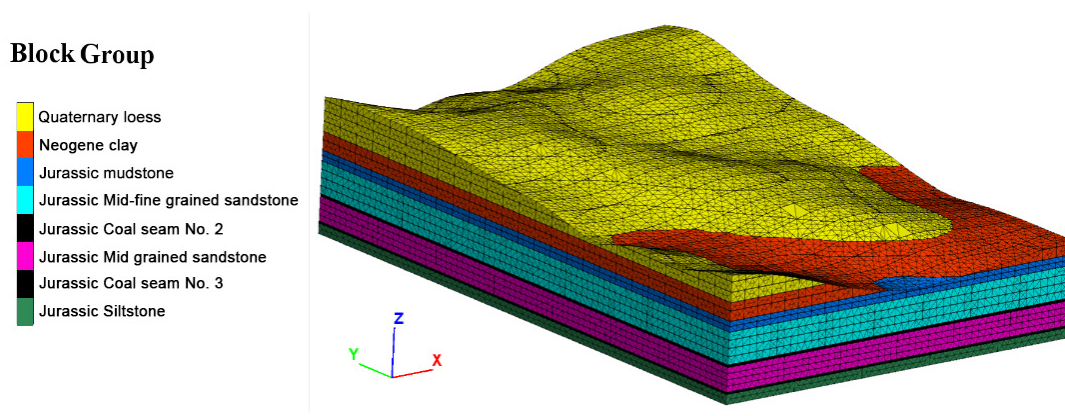


Figure 8. Model of the study area 4.1 identification of water-conducting fractured zone.

Figure 9a shows the plastic diagram of the mined panel 30302, where the caving production ratio of panel 30302 is 5 times (10 m), and the ratio of the height of the water-conducting fractured zone to the mining height is 25 times (50 m) without the mining of panel 20202. Affected by mining, obvious cracks developed in the loose layer of the Quaternary system on the surface. Figure 9b shows the plastic diagram of mined panels 30302 after panel 20202 was mined; the overlying strata were affected by multiple mining disturbances, resulting in a higher water-conducting fractured zone.

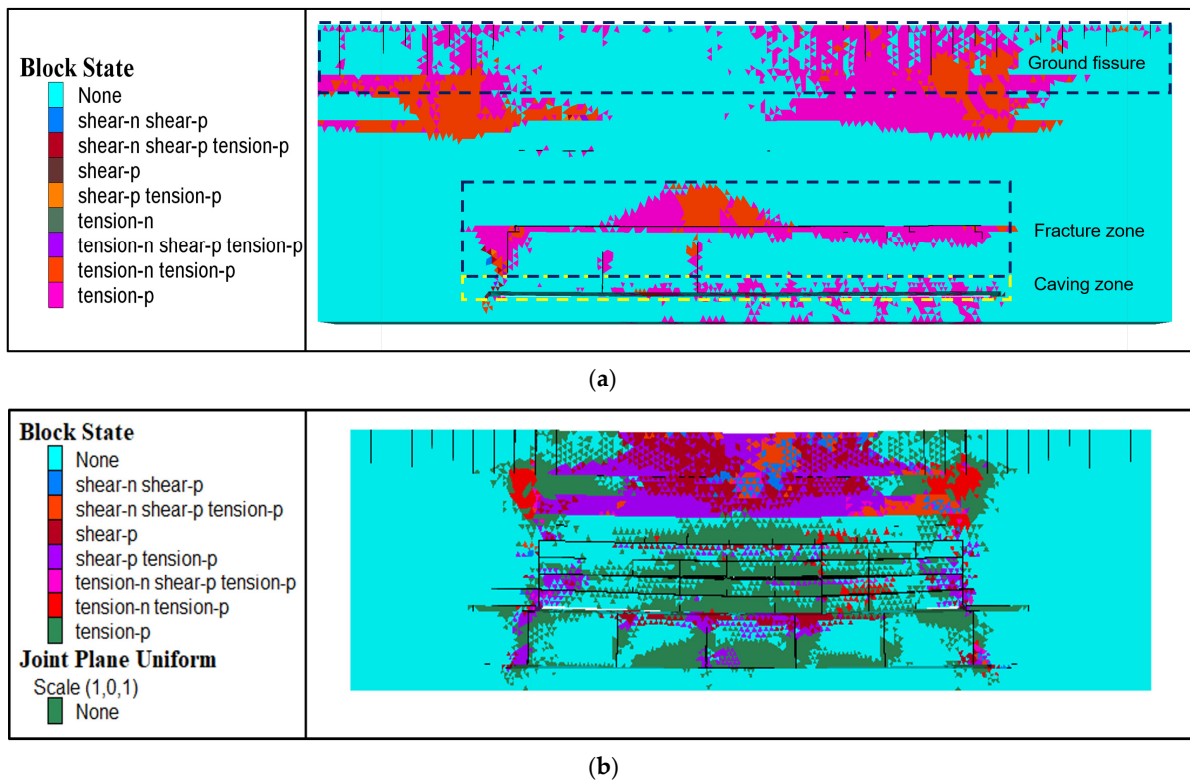


Figure 9. Simulation of mining in panel 30302. (a) Without mining panel 20202. (b) After mining panel 20202.

On-Site Monitoring

Figure 10 shows optical fiber monitoring data. It was obvious that the maximum microstrain increased when panel 30302 was excavated. Furthermore, when the mining point in panel 30302 approached the monitoring of boreholes, the microstrain increased dramatically (Figure 10a-Trial No. 11 and Figure 10b-Trial No. 5). Moreover, due to the growth of the water-conducting fractured zone, the fiber was damaged when the mining position went through the monitoring borehole. (Figure 10b-Trial No. 8).

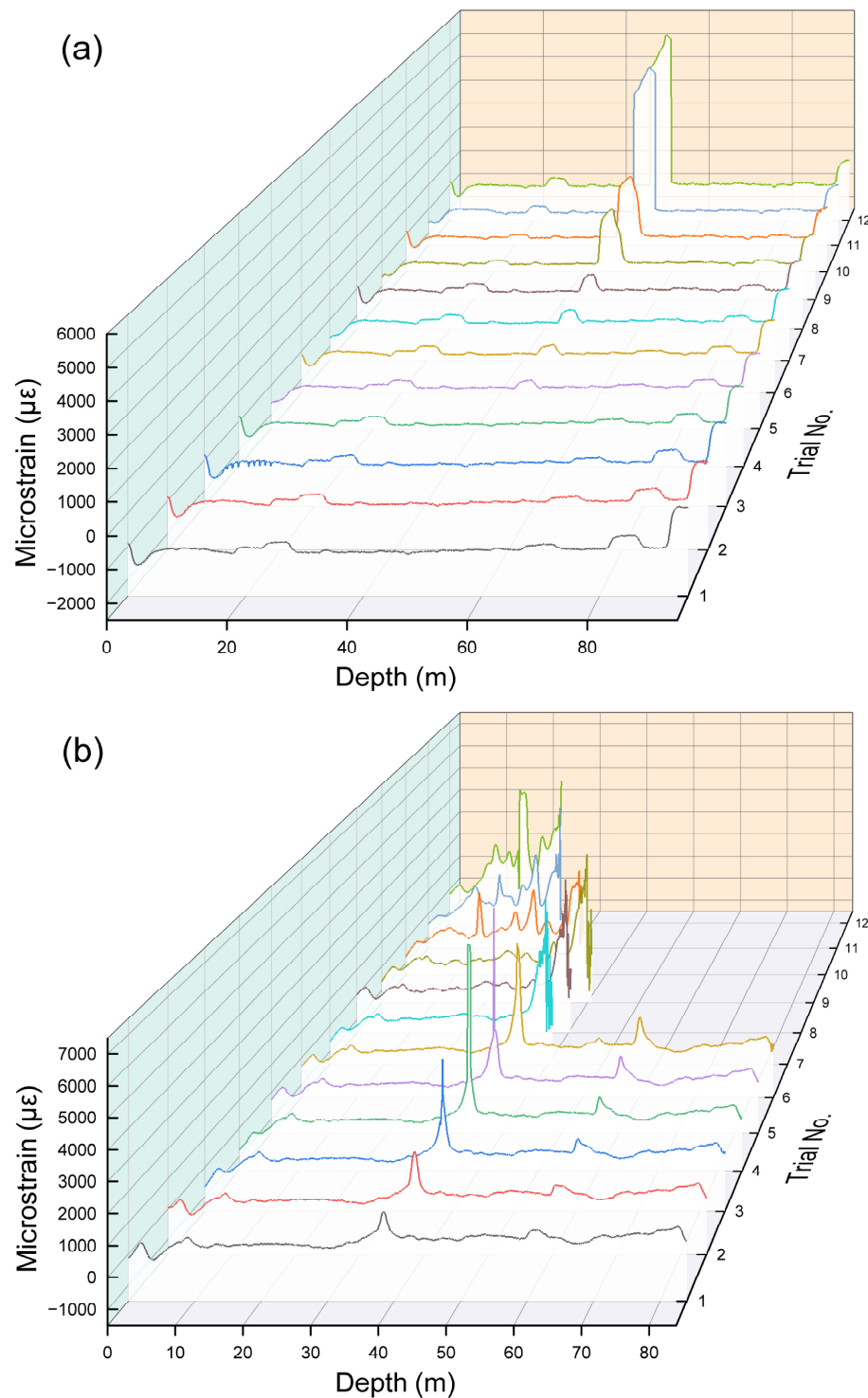


Figure 10. Optical fiber monitoring of panel 30302. (a) Monitoring borehole No. 2. (b) Monitoring borehole No. 1.

Figure 11a shows that the depth of the first peak from the bottom to the top of optical-fiber monitoring is 91 m, 11 m away from the roof of panel 30302; therefore, it can be judged that the caving zone of panel 30302 at monitoring borehole No. 2 is 11 m. The maximum tensile strain is located at a depth of 50 m, 52 m away from the roof of panel 30302, which is considered the boundary of the water-flowing fractured zone of panel 30302. In addition, the depth of 22 m is the boundary of the superimposed water-flowing fractured zone of panels 20202 and 30302. Similarly, the height of the caving zone at monitoring borehole No. 1 is 14 m. The depth of the boundary of the water-conducting fractured zone in monitoring borehole No. 1 is 51 m. The depth of 20 m is the boundary of the superimposed water-flowing fractured zone of panels 20202 and 30302 at monitoring borehole No. 1 (Figure 11b).

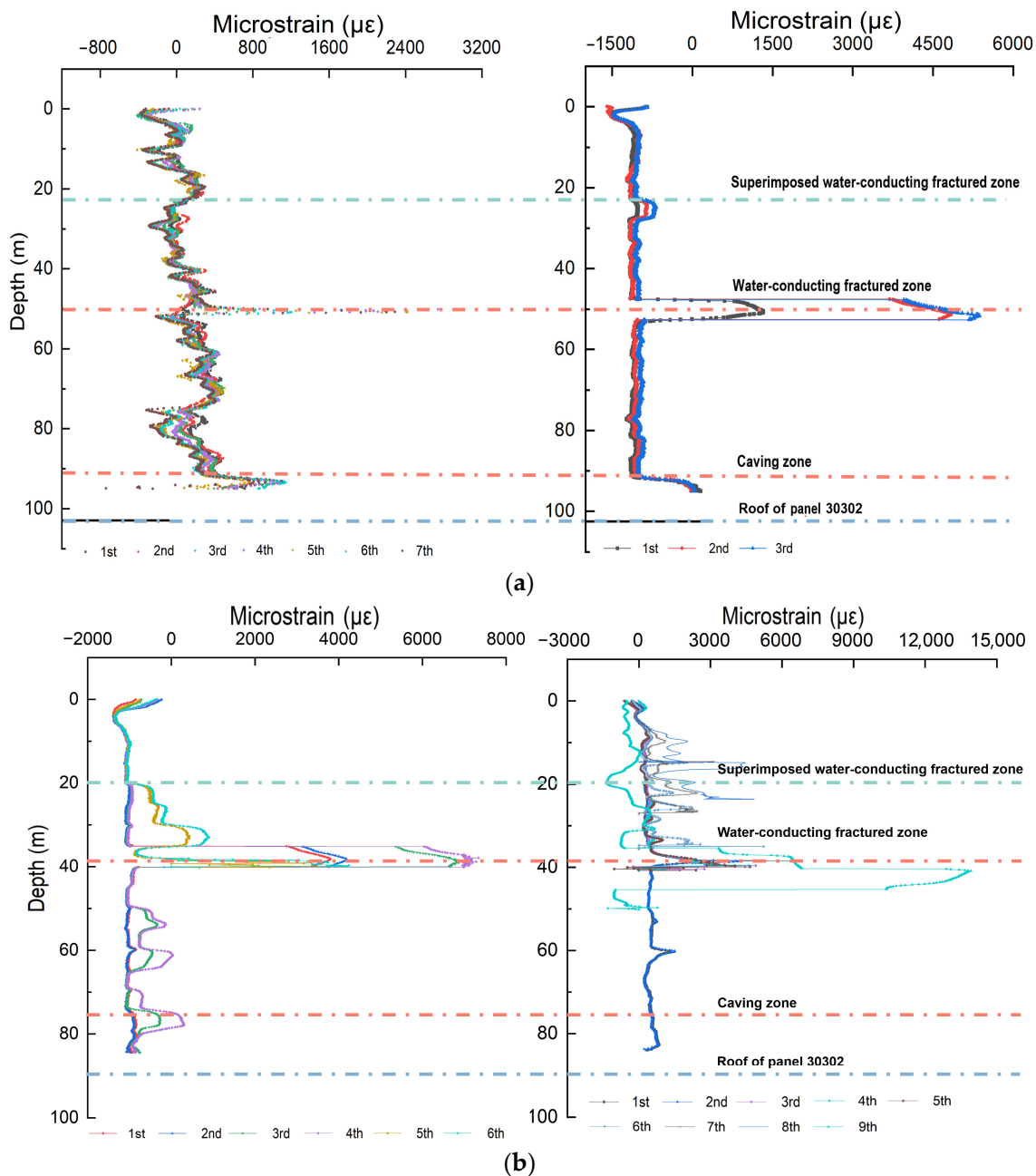


Figure 11. Analysis of optical fiber monitoring data. (a) Borehole No. 2. (b) Borehole No. 1.

The optical fiber data of monitoring boreholes No. 1 and No. 2 suggest that the height of the caving zone in panel 30302 is 11–14 m, the height of the water-flowing fractured zone is 51–52 m, and the superimposed water-flowing fractured zone is 70–80 m.

The MAD at 36 m of monitoring borehole No. 1 (Table 5) is 1559, while it is 887 at 56 m of monitoring borehole No. 2 (Table 6). Monitoring boreholes No. 1 and No. 2 had maximum values of 6367 (4.1 MAD) and 4159 (4.7 MAD), respectively, both of which are less than 5 MAD.

Table 5. Partial monitoring data of borehole No. 1.

Depth (m)	Trail No.								
	1	2	3	4	5	6	7	8	
35.7		−1018	−1016	−1016	−644	−322	−301	7	77
35.8		−1024	−1027	−1035	−634	−310	−273	34	110
35.9		−1022	−1045	−1040	−628	−308	−257	56	130
36		−1046	−1057	−1046	−616	−297	−245	82	139
36.1		−1034	−1047	−1026	−610	−271	−233	95	162
36.2		−1043	−1035	−1039	−596	−267	−233	91	174
36.3		−1042	−1041	−1022	−583	−271	−204	120	193
	9	9	10	11	12	13	14	15	16
35.7		555	689	1427	1457	2962	3295	5494	6168
35.8		592	725	1463	1469	2986	3339	5511	6195
35.9		627	744	1501	1486	3017	3344	5540	6208
36		628	764	1502	1525	3031	3379	5566	6248
36.1		640	785	1528	1541	3055	3390	5601	6290
36.2		667	793	1549	1563	3104	3418	5634	6323
36.3		659	824	1575	1586	3117	3451	5690	6367

Table 6. Partial monitoring data of borehole No. 2.

Depth (m)	Trail No.								
	1	2	3	4	5	6	7	8	
49.7		−1050	−1156	−1086	−1136	−1103	−843	−810	−625
49.8		−1077	−1159	−1086	−1127	−1093	−825	−797	−625
49.9		−1068	−1172	−1098	−1128	−1100	−833	−782	−630
50		−1099	−1183	−1094	−1136	−1087	−835	−783	−615
50.1		−1100	−1151	−1090	−1100	−1086	−837	−793	−640
50.2		−1065	−1177	−1085	−1107	−1091	−811	−771	−620
50.3		−1084	−1159	−1083	−1100	−1086	−829	−786	−637
	9	10	11	12	13	14	15		
49.7		−422	947	1187	4376	4563	4256	4175	
49.8		−464	954	1202	4409	4614	4225	4150	
49.9		−438	986	1218	4461	4637	4195	4116	
50		−483	977	1219	4494	4674	4170	4105	
50.1		−434	1008	1261	4533	4718	4128	4151	
50.2		−428	1035	1286	4561	4735	4121	4111	
50.3		−408	1047	1297	4592	4763	4106	4159	

According to the monitoring results of the parallel network electrical method (Figure 12), there was no geophysical anomaly in the monitoring area, and the height of the water-flowing fractured zone during mining was within the normal range. As a result, there was no danger of water inrush.

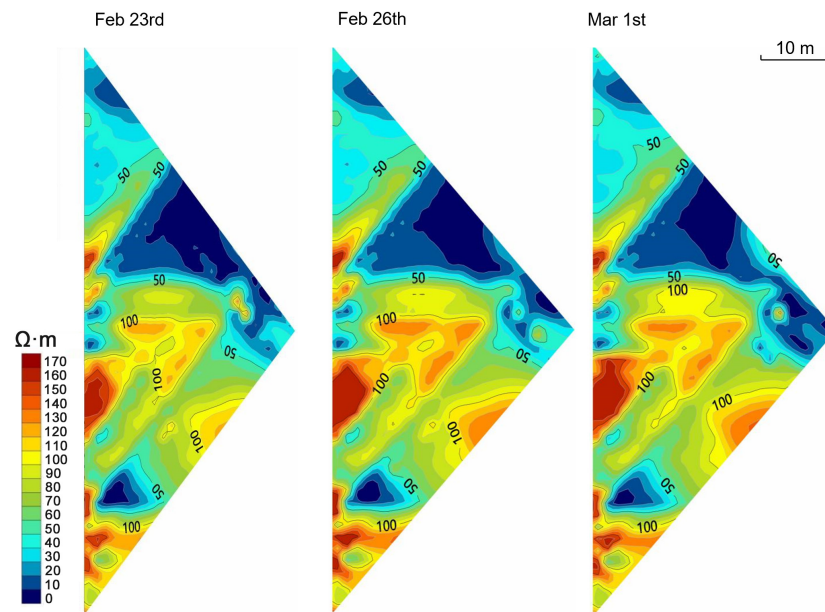


Figure 12. Profile of apparent resistivity in monitoring borehole No. 1.

5. Discussion

5.1. Re-Verification of Modelling

Panel 1304 of the Zhaoxian coal mine in Shaanxi Province was chosen to test the applicability of the early warning-model because there was no water inrush during the study period at the Yanghuopan coal mine [41]. Its stratum was comparable to that of the study area, and the mined coal seam was also Jurassic coal seam No. 3. G3's observation well was 424 m away from the panel's water inrush position, while G4's was 1116 m. Water inrush began at 11 a.m. on 28 March 2020, with a water inflow of 3 m³/h. The water inflow reached 40 m³/h at 2 p.m. on the 29th, with a maximum of 280 m³/h. Figure 13 shows water level monitoring data from G3 and G4 observation wells. The two water level observation wells' water levels started to decline quickly after 22 March, as seen in Figure 13.

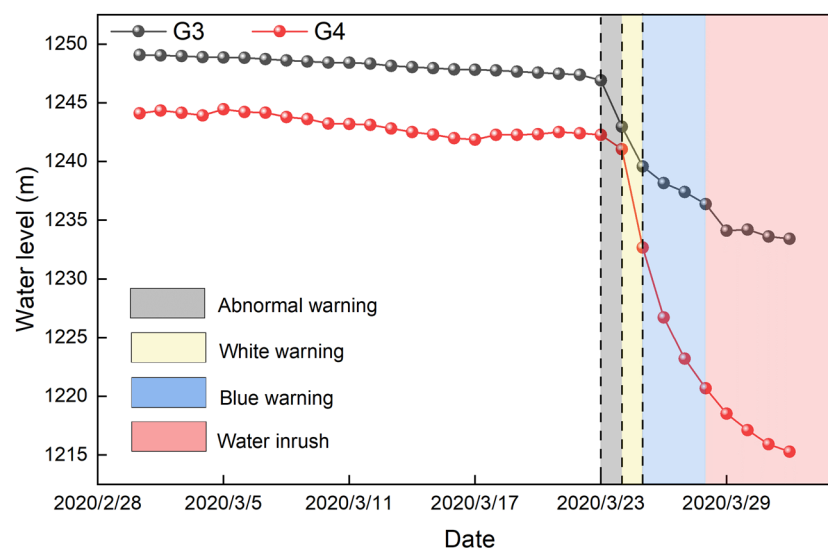


Figure 13. Water level in observation wells of G3 and G4.

Table 7 displays the analysis results of a real-time early-warning model in a single indicator with short-time mode. Only the indicators for monitoring water levels were

gathered on-site; it was evident that if a single-factor early-warning system was used, a series of anomalous signals would be sent, such as from 9 March to 17 March, but many factors also showed that there was no concern. Even if there was only a water level monitoring indication, the multi-indicator monitoring system provided a white warning on 24 March and a blue alert on 25 March until the water inrush on 28 March.

Table 7. Monitoring data and warning grade of G3 and G4.

Date(y/m/d)	Water Level of G3	$ Z - \bar{Z}_s $	Single Indicator	Water Level of G4	$ Z - \bar{Z}_s $	Single Indicator	Multiple Indicators
2020/3/8	1248.61	0.30	Riskless	1243.78	0.41	Riskless	Riskless
2020/3/9	1248.52	0.33	Riskless	1243.62	0.52	Abnormal	Riskless
2020/3/10	1248.42	0.35	Riskless	1243.23	0.81	Abnormal	Riskless
2020/3/11	1248.41	0.28	Riskless	1243.2	0.71	Abnormal	Riskless
2020/3/12	1248.33	0.29	Riskless	1243.12	0.69	Abnormal	Riskless
2020/3/13	1248.14	0.41	Riskless	1242.81	0.81	Abnormal	Riskless
2020/3/14	1248.04	0.41	Riskless	1242.51	0.91	Abnormal	Riskless
2020/3/15	1247.95	0.40	Riskless	1242.29	0.89	Abnormal	Riskless
2020/3/16	1247.85	0.41	Riskless	1241.99	0.98	Abnormal	Riskless
2020/3/17	1247.81	0.35	Riskless	1241.86	0.88	Abnormal	Riskless
2020/3/18	1247.76	0.32	Riskless	1242.27	0.27	Riskless	Riskless
2020/3/19	1247.66	0.32	Riskless	1242.27	0.14	Riskless	Riskless
2020/3/20	1247.57	0.32	Riskless	1242.33	0.04	Riskless	Riskless
2020/3/21	1247.48	0.33	Riskless	1242.51	0.29	Riskless	Riskless
2020/3/22	1247.38	0.35	Riskless	1242.4	0.18	Riskless	Riskless
2020/3/23	1246.91	0.73	Abnormal	1242.27	0.04	Riskless	Riskless
2020/3/24	1242.96	4.55	Medium-risk	1241.05	1.22	Low-risk	White
2020/3/25	1239.57	7.25	High-risk	1232.67	9.49	High-risk	Blue
2020/3/26	1238.16	7.49	High-risk	1226.72	14.07	Extremely high-risk	Blue
2020/3/27	1237.4	6.89	High-risk	1223.21	15.35	Extremely high-risk	Blue
2020/3/28	1236.37	6.47	High-risk	1220.68	15.15	Extremely high-risk	Blue
2020/3/29	1234.11	7.14	High-risk	1218.52	14.19	Extremely high-risk	Blue
2020/3/30	1234.2	5.15	High-risk	1217.12	12.18	Extremely high-risk	Blue
2020/3/31	1233.61	3.93	Medium-risk	1215.92	9.79	High-risk	Blue
2020/4/1	1233.42	2.78	Medium-risk	1215.28	6.84	High-risk	Blue

Then, a stochastic oscillator was used to analyze the monitoring data of the water level. Before applying this method, the set value of the calculation period was first defined in order to calculate the raw stochastic value (RSV). Because this was the first time the Stochastic oscillator was applied to mining water hazard analysis, determining the right value was impossible; thus, it is evaluated in 3, 5, 7, 10, 15, and 20 days (Figures 14 and 15). When the three lines connected, it usually implied that the present water level trend was about to change. When the value of the J line broke through 100, it meant that the water level would suddenly drop, indicating a high possibility of water inrush. By comparing different periods, the indicator was more sensitive to water level data when the computation period was less than 7 days, such as 3 or 5 days (Figure 15a, b), even resulting in unnecessary false alarms. When the period exceeds 10 days, such as 15 or 20 days, the indicator becomes insensitive to the data and could even overlook the early-warning signal. Furthermore, a 7-day period was best suited to the conditions of the study region.

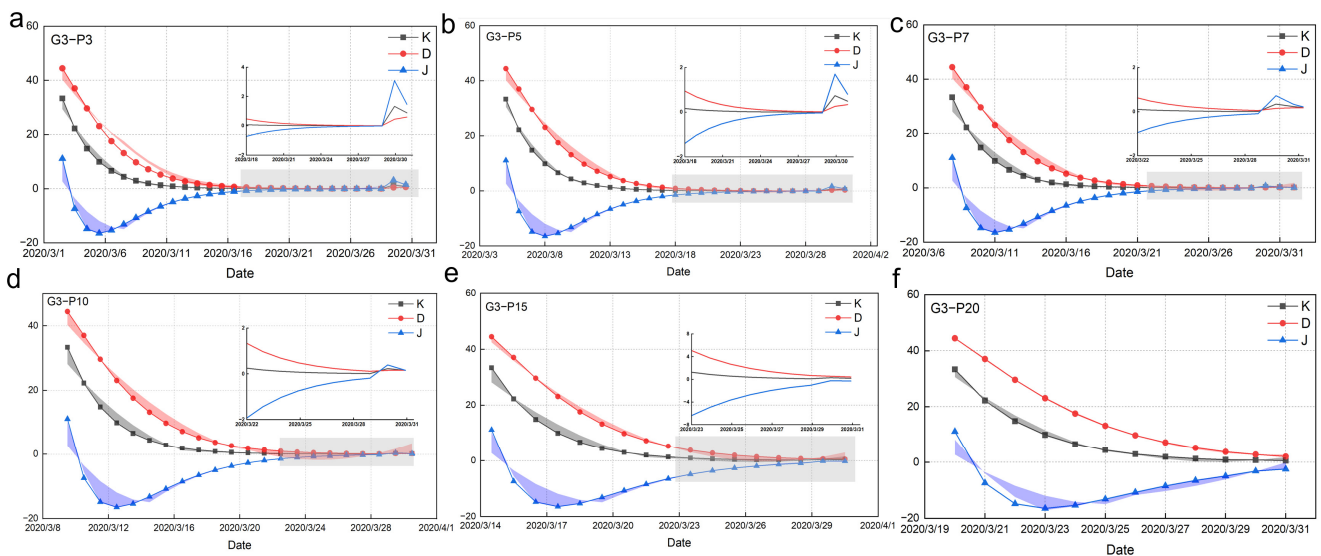


Figure 14. Stochastic oscillator of water level in observation well G3 in the following periods: (a) 3 days, (b) 5 days, (c) 7 days, (d) 10 days, (e) 15 days, and (f) 20 days.

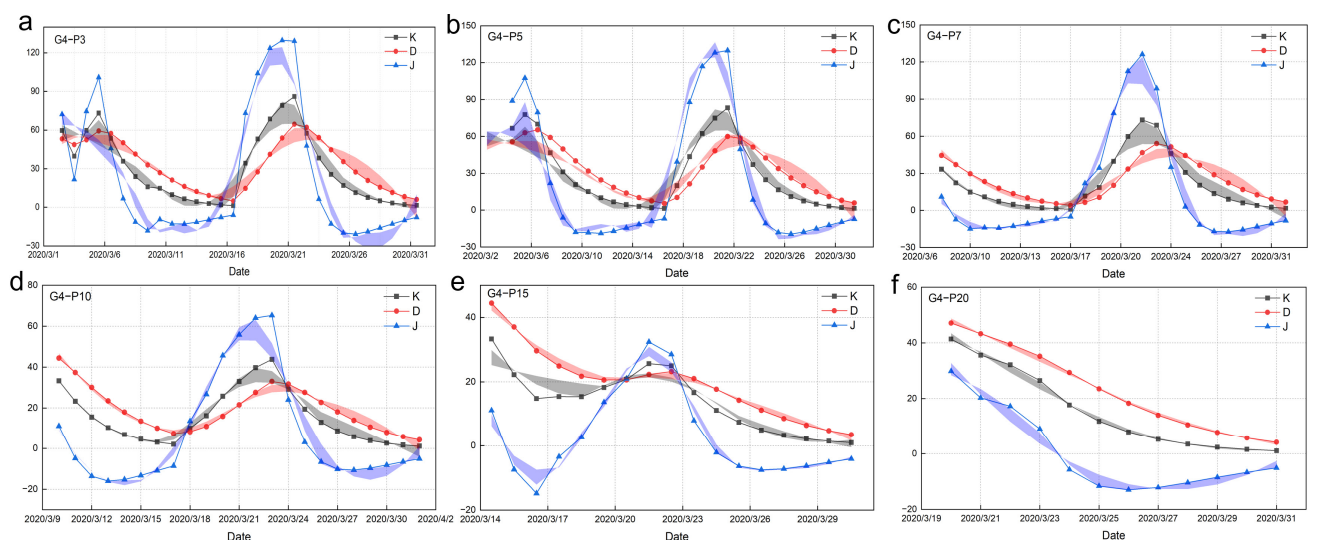


Figure 15. Stochastic oscillator of water level in observation well G4 in the following periods: (a) 3 days, (b) 5 days, (c) 7 days, (d) 10 days, (e) 15 days, and (f) 20.

As shown in Figure 13, the water levels in the two observation wells plummeted after water inrush, but when combined with Figures 14 and 15, it was clear that, while the water source at the position of observation well G3 had always shown a downward trend, the water source at the position of observation well G4 was more closely related to the mining water inrush, which can provide an effective early warning through the Stochastic oscillator for this disassembly of the mining water.

We can deduce that panel 1304 experienced bed separation during mining on about 16th March. The water near the water inrush point (G3) began gathering in the bed separation, affecting the water source near the observation well G4. During this time, the single-factor early-warning system already sent an ‘Abnormal’ alert due to an abnormal decline in the water level in observation well G3. A certain amount of water was gathered in the bed separation on 24 March. When the J-line dropped and the three lines connected (Figure 15c), the water contained at that time progressively reached the bearing limit of bed separation. In conjunction with the current water level variations in two monitoring wells, our multi-factor early warning-system also issued a ‘White’ early warning at this time and

gradually increased the early-warning level. It can be inferred from (Table 7) that there was a substantial probability that mine water inrush could occur.

After the accident investigation, it was confirmed that the water inrush was indeed a water disaster in the bed separation. Using this early-warning model, early-warning information could be received three days before the occurrence of this water disaster accident, reducing water disaster losses and even checking the hidden threats of the accident in advance to avoid disasters.

5.2. Monitoring Indicators

The damage range and degree of overlying strata in the panel directly determine the safety of coal mining. It is a necessary condition for mine water inrush whether the water-conducting fractured zone can conduct the overlying aquifer. The method of parallel network electricity and Brillouin optical time domain reflectometer is adopted to identify water-conducting fracture zones in real-time. The degree of hazard and risk posed by an inrush is usually proportional to the amount of water, the water pressure, and the pumping capacity of the mine [44]. The rock mass temperature near the water passage and the water temperature of the coal seam fissure water are abnormal when the water from the coal seam roof enters the water-resisting layer through the fissure, so the temperature clearly changes in the early stage of water inrush. By monitoring the water temperature of the overlying aquifer, the possibility of water inrush can be predicted. In addition, mine hydrochemistry can also warn of a water inrush. Especially in the process of coal mining under the thin bedrock and thick loose layer, the water quality in the loose layer is different from that in the coal aquifer. As a result, monitoring mine water quality can provide a foundation for determining water inrush. The early-warning model adopts optical fiber, the electricity method, water temperature, and water level as early-warning monitoring factors. Then, it can be decided whether to add a hydrochemical indicator according to the application of the model.

During this model's development, we believed that the multi-indicator early-warning model was not an upgrade over a single-factor early-warning model but rather a perfection of the single-factor early-warning model. A single-factor warning only selects a single factor for monitoring, although it has been subdivided into short-time and long-time modes. It is not coupled with other factors for monitoring, compared with multi-indicators, which leads to its weak anti-interference performance, while multiple monitoring indicators are comprehensively considered in the multi-indicator early-warning model. The mutual verification of many parameters can lessen the alert triggered by the unintended fluctuation of a single factor in the early-warning model and increase its accuracy.

Additionally, the forecast grade should be the average value or the value that is more closely connected if the same factor comprises several monitoring data, such as multiple monitoring boreholes in the monitoring site.

5.3. Development of Early-Warning Platform

The objectives of the water inrush warning platform are as follows: master the real-time monitoring information of each monitoring index, such as microstrain, apparent resistivity, water level, water quantity, and water temperature; generate various hydrological monitoring data reports and automatically calculate short-term and long-term averages; evaluate the current risk level by comparing the real-time monitoring values with the threshold parameters; finally, according to the warning level, a real-time response can be made to give an alarm to guide people to avoid risks.

The initial development of the early-warning platform is divided into four parts (Figure 16), namely the graphical user interface (GUI) design, data input, analysis, and output. GUI, as a graphical user interface for computer operation, is a dialogue interface between the computer and its users. In data acquisition, the platform should be able to identify and remove data with accidental errors. Then, the platform can display the monitoring curve, calculate the threshold in real-time, and obtain the current state of the

panel. The final quantitative output of the early-warning model is the risk value (RK), obtained according to the abnormal situation of the monitoring values of each index.

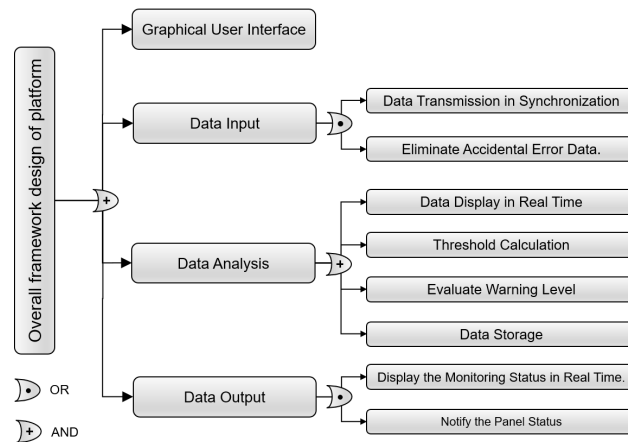


Figure 16. Framework of the early-warning platform.

The platform was initially created utilizing the Python programming language and the early-warning model creation method. To actualize the platform’s functionality, the platform’s code incorporates third-party Python libraries such as Matplotlib, numPy, time, xlrd, csv, and so on. At the moment, the platform can analyze data based on its countdown data and make recommendations on water inrush risk. Figure 17 depicts the interface platform as well as some source codes.

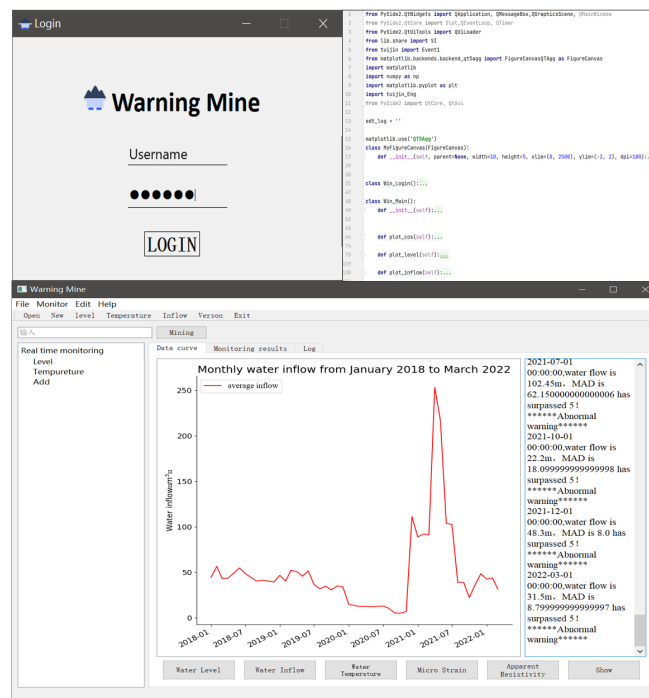


Figure 17. ‘Warning Mine’ program.

5.4. Limitations and Further Study

Because of the relentless and continual changes in the ground and subsurface conditions caused by mining, the occurrence of water inrushes is a dynamic process. Water inrushes are difficult to predict with 100 percent confidence in terms of timing and extent [39]. There is a paucity of data to adequately identify the threshold due to the short

monitoring and tracking times in the study area. Obtaining adequate data after applying the model can make the early-warning model's threshold more acceptable for the mining location. The thresholds and boundary values of the above models are only based on existing data at present and still need to be improved by collecting and supplementing relevant monitoring data to improve the accuracy and effectiveness of the early-warning model. The monitored indicators are constrained by the available monitoring conditions in the mining region. Based on their mining characteristics and the established model framework, the other mining locations can select relevant monitoring indicators. Furthermore, we aim to also keep improving the platform and enriching its features.

Along with the early-warning model, we also tested the stochastic oscillator's capacity for early warning in mine water disasters. The stochastic oscillator, a statistical technique used in the financial sector, shows its applicability in early warning of mine water inrush. However, in order to be more suitable for early warning of mine water inrush, to achieve more precise, sensitive, and objective early warning, and to escort mine production safety, it must be further improved in accordance with the characteristics of coal mine disasters. This will be the focus of future research.

6. Conclusions

The main conclusions and findings are summarized as follows:

- (1) An early-warning model of water inrush is established, which is dominated by the distance between the mining position and the monitoring borehole. The model mainly includes three parts as follows: the development and identification of a water-conducting fracture zone, the early warning of multi-indicators, and a stochastic oscillator.
- (2) In the dependence of sensitivity analysis, the monitoring indicators are obtained, and the warning modes are determined. The indicators of water level, temperature, and apparent resistivity adopt variable value mode, and water inflow adopts a variable amplitude mode.
- (3) The model was applied in the Yushen mining areas' panel 30302 of the Yanghuopan coal mine and panel 1304 of the Zhaoxian coal mine. The results show that the model can provide a reference for the early warning of water inrush, especially for the water disaster in bed separation.

Author Contributions: J.L. was involved in conceptualization, methodology, formal analysis, literature search, data curation, investigation, resources, visualization, writing—original draft, writing—review and editing. W.S. helped in project administration, funding acquisition, supervision. G.C. contributed to supervision. H.R. and X.L. helped in project administration. All authors have read and agreed to the published version of the manuscript.

Funding: This research was funded by the National Natural Science Foundation of China with Grant No. 42130706.

Data Availability Statement: Data are contained within the article.

Conflicts of Interest: Author Hujun Ren and Xibin Li were employed by the company China Coal Hydrogeological Bureau Group Company. The remaining authors declare that the research was conducted in the absence of any commercial or financial relationships that could be construed as a potential conflict of interest.

References

1. Liang, Y.K.; Sui, W.H.; Jiang, T.; Shen, X.Y. Experimental Investigation on the Transport Behavior of a Sand/Mud/Water Mixture Through a Mining-Induced Caving Zone. *Mine Water Environ.* **2022**, *41*, 629–639. [[CrossRef](#)]
2. Sui, W.H.; Wang, D.D.; Sun, Y.J.; Yang, W.F.; Xu, Z.M.; Feng, L. Mine hydrogeological structure and its responses to mining. *J. Eng. Geol.* **2019**, *27*, 21–28. (In Chinese with abstract in English) [[CrossRef](#)]
3. Jin, D.W.; Zheng, G.; Liu, Z.B.; Liu, Y.F.; Pang, X.Q. Real-time monitoring and early warning techniques of water inrush through coal floor. *Procedia Earth Planet. Sci.* **2011**, *3*, 37–46. [[CrossRef](#)]
4. Qian, Z.W.; Jiang, Z.Q.; Guan, Y.Z.; Yue, N. Mechanism and Remediation of Water and Sand Inrush Induced in an Inclined Shaft by Large-Tonnage Vehicles. *Mine Water Environ.* **2018**, *37*, 849–855. [[CrossRef](#)]

5. Zadkov, D.A.; Gabov, V.V.; Babyr, N.V.; Stebnev, A.V.; Teremetskaya, V.A. Adaptable and energy-efficient powered roof support unit. *Min. Information Anal. Bull.* **2022**, *6*, 46–61. [[CrossRef](#)]
6. Gabov, V.V.; Zadkov, D.A.; Babyr, N.V.; Xie, F.W. Nonimpact rock pressure regulation with energy recovery into the hydraulic system of the longwall powered support. *Eurasian Min.* **2021**, *2021*, 55–59. [[CrossRef](#)]
7. Wu, J.S.; Xu, S.D.; Zhou, R.; Qin, Y.P. Scenario analysis of mine water inrush hazard using Bayesian networks. *Saf. Sci.* **2016**, *89*, 231–239. [[CrossRef](#)]
8. Jin, D.W.; Zhang, G.; Liu, Z.B.; Chen, B.H. Real time monitoring and early warning of water inrush in a coal seam floor: A case study. *Mine Water Environ.* **2021**, *40*, 378–388. [[CrossRef](#)]
9. Liu, S.L.; Liu, W.T.; Huo, Z.C.; Song, W.C. Early warning information evolution characteristics of water inrush from floor in underground coal mining. *Arab. J. Geosci.* **2019**, *12*, 30. [[CrossRef](#)]
10. Zhu, Z.K.; Xu, Z.M.; Sun, Y.J. Critical water inrush monitoring index and early-warning model of mine water disaster. *Saf. Coal Mines* **2014**, *45*, 170–172. (In Chinese with abstract in English) [[CrossRef](#)]
11. Li, Y.H.; Bai, J.B.; Yan, W.; Wang, X.Y.; Wu, B.W.; Liu, S.G.; Xu, J.; Sun, J.X. Risk early warning evaluation of coal mine water inrush based on complex network and its application. *Adv. Civ. Eng.* **2021**, *2021*, 1–13. [[CrossRef](#)]
12. Liu, B.; Li, S.C.; Nie, L.C.; Wang, J.; Li, L.P.; Liu, Z.Y.; Song, J. Research on simulation of mine water inrush real-time monitoring of using electrical resistivity constrained inversion imaging method. *J. China Coal Soc.* **2012**, *37*, 1722–1731. [[CrossRef](#)]
13. Zhao, J.Y.; Liu, W.T.; Shen, J.J.; Xu, M.H.; Sasmito, A.P. A real-time monitoring temperature-dependent risk index for predicting mine water inrush from collapse columns through a coupled thermal-hydraulic-mechanical model. *J. Hydrol.* **2022**, *607*, 1–22. [[CrossRef](#)]
14. Sun, Y.J.; Zhang, L.; Xu, Z.M.; Chen, G.; Zhao, X.M.; Li, X.; Gao, Y.T.; Zhang, S.G.; Zhu, L.L. Multi-field action mechanism and research progress of coal mine water quality formation and evolution. *J. China Coal Soc.* **2022**, *47*, 423–437. (In Chinese with abstract in English)
15. Wang, S.; Li, L.P.; Cheng, S.; Yang, J.Y.; Jin, H.; Gao, S.; Wen, T. Study on an improved real-time monitoring and fusion prewarning method for water inrush in tunnels. *Tunn. Undergr. Space Technol.* **2021**, *112*, 1–10. [[CrossRef](#)]
16. Xu, Z.M.; Sun, Y.J.; Gong, S.Y.; Zhu, Z.K. Monitoring and numerical simulation of formation of water inrush pathway caused by coal mining above confined water with high pressure. *Chin. J. Rock Mech. Eng.* **2012**, *31*, 1698–1704. (In Chinese with abstract in English)
17. Sui, W.H. Active prevention and control of water-sand mixture inrush with high potential energy due to mining based on structural hydrogeology. *J. Eng. Geol.* **2022**, *30*, 101–109. (In Chinese with abstract in English). [[CrossRef](#)]
18. Dong, S.N.; Wang, J.M.; Gao, Z.L.; He, Z.L. Development and application of monitoring system for water inrush from coal seam floor. *Min. Saf. Environ. Prot.* **1998**, *6*, 12–14. (In Chinese)
19. Chitsazan, M.; Heidari, M.; Ghobadi, M.H.; Torabi-Kaveh, M.; Mohammadi-Behzad, H.R.; Kavousi, A.R. The study of the hydrogeological setting of the Chamshir Dam site with special emphasis on the cause of water salinity in the Zohreh River downstream from the Chamshir Dam (southwest of Iran). *Environ. Earth Sci.* **2012**, *67*, 1605–1617. [[CrossRef](#)]
20. Wang, X.; Xu, Z.M.; Sun, Y.J.; Zheng, J.M.; Zhang, C.H.; Duan, Z.W. Construction of multi-factor identification model for real-time monitoring and early warning of mine water inrush. *Int. J. Min. Sci. Technol.* **2021**, *31*, 853–866. [[CrossRef](#)]
21. Liu, J.B.; Si, Y.T.; Wei, D.C.; Shi, H.X.; Wang, R. Developments and prospects of microseismic monitoring technology in underground metal mines in China. *J. Cent. South Univ.* **2021**, *28*, 3074–3098. [[CrossRef](#)]
22. Ma, K.; Sun, X.Y.; Tang, C.A.; Wang, S.J.; Yuan, F.Z.; Peng, Y.L.; Liu, K. An early warning method for water inrush in Dongjiahe coal mine based on microseismic moment tensor. *J. Cent. South Univ.* **2020**, *27*, 3133–3148. [[CrossRef](#)]
23. Bismayer, U. Early warning signs for mining accidents: Detecting crackling noise. *Am. Mineral.* **2017**, *102*, 3–4. [[CrossRef](#)]
24. Tu, W.F.; Li, L.P.; Shang, C.S.; Liu, S.; Zhu, Y.Z. Comprehensive risk assessment and engineering application of mine water inrush based on normal cloud model and local variable weight. *Energy Sources Part A Recovery Util. Environ. Eff.* **2019**, *41*, 1–16. [[CrossRef](#)]
25. Fang, B. Method for quickly identifying mine water inrush using convolutional neural network in coal mine safety mining. *Wirel. Pers. Commun.* **2021**, *127*, 945–962. [[CrossRef](#)]
26. Yang, W.F.; Xia, X.H.; Pan, B.L.; Gu, C.S.; Yue, J.G. The fuzzy comprehensive evaluation of water and sand inrush risk during underground mining. *J. Intell. Fuzzy Syst. Appl. Eng. Technol.* **2016**, *30*, 2289–2295. [[CrossRef](#)]
27. Sun, W.B.; Xue, Y.C. An improved fuzzy comprehensive evaluation system and application for risk assessment of floor water inrush in deep mining. *Geotech. Geol. Eng.* **2019**, *37*, 1–11. [[CrossRef](#)]
28. Kumar, A.; Kumar, D.; Singh, A.K.; Ram, S.; Kumar, R.; Gautam, A.; Singh, R.; Singh, A.K. Roof sagging limit in an early warning system for safe coal pillar extraction. *Int. J. Rock Mech. Min. Sci.* **2019**, *123*, 104131. [[CrossRef](#)]
29. Builes, J.A.J.; Acero, A.R.; Cano, A.M. Red de sensores inalámbricos para el monitoreo de alertas tempranas en minas subterráneas: Una solución a la problemática de atmósferas explosivas en la minería de carbón en Colombia. *Rev. Científica Ing. Desarro.* **2013**, *31*, 227–250.
30. Zhao, L.; Ting, R.; Wang, N.B. Groundwater impact of open cut coal mine and an assessment methodology: A case study in NSW. *Int. J. Min. Sci. Technol.* **2017**, *27*, 861–866. [[CrossRef](#)]
31. Hebblewhite, B. Fracturing, caving propagation and influence of mining on groundwater above longwall panels—A review of predictive models. *Int. J. Min. Sci. Technol.* **2020**, *30*, 49–54. [[CrossRef](#)]

32. Gao, L.; Gong, Y.H.; Yu, Y.J.; Qian, X.S.; Qin, P.F. Development and application of distributed optical fiber inclinometer based on Brillouin scattering time domain reflection measurement technology. *Sci. Technol. Eng.* **2017**, *17*, 81–85. (In Chinese with abstract in English)
33. Chu, Y.F.; Hahn, J. Necessary condition for applying experimental design criteria to global sensitivity analysis results. *Comput. Chem. Eng.* **2013**, *48*, 280–292. [[CrossRef](#)]
34. Wang, Y.; Yang, W.F.; Ming, L.; Liu, X. Risk assessment of floor water inrush in coal mines based on secondary fuzzy comprehensive evaluation. *Int. J. Rock Mech. Min. Sci.* **2012**, *52*, 50–55. [[CrossRef](#)]
35. Liang, J.X.; Sui, W.H. Sensitivity analysis of anchored slopes under water level fluctuations: A case study of Cangjiang Bridge—Yingpan slope in China. *Appl. Sci.* **2021**, *11*, 7137. [[CrossRef](#)]
36. Song, X.M.; Zhang, J.Y.; Zhan, C.S.; Xuan, Y.Q.; Ye, M.; Xu, C.G. Global sensitivity analysis in hydrological modeling: Review of concepts, methods, theoretical framework, and applications. *J. Hydrol.* **2015**, *523*, 739–757. [[CrossRef](#)]
37. Chen, J.C.; Zhou, Y.; Wang, X. Profitability of simple stationary technical trading rules with high-frequency data of Chinese Index Futures. *Phys. A-Stat. Mech. Its Appl.* **2018**, *492*, 1664–1678. [[CrossRef](#)]
38. Wu, S. Application of Cluster Analysis in Stock Selection in United States Stock Market. In Proceedings of the 2020 11th International Conference on E-Education, E-Business, E-Management, and E-Learning (IC4E 2020), Osaka, Japan, 10–12 January 2020; pp. 310–313. [[CrossRef](#)]
39. Ye, F.; Zhang, L.; Zhang, D.; Fujita, H.; Gong, Z. A novel forecasting method based on multi-order fuzzy time series and technical analysis. *Inf. Sci.* **2016**, *367*, 41–57. [[CrossRef](#)]
40. Shou, M.H.; Wang, Z.X.; Li, D.D.; Zhou, Y.T. Forecasting the price trends of digital currency: A hybrid model integrating the stochastic index and grey Markov chain methods. *Grey Syst.-Theory Appl.* **2021**, *11*, 22–45. [[CrossRef](#)]
41. Xu, J.P.; Zhou, Y.; Pu, Z.H.; Pang, S.Y. Calculation method of separated water accumulation in the process of separated water inrush and its forecast: Taking the water inrush at 1304 working face of Zhaoxian Coal Mine in Shaanxi Province as an example. *J. China Coal Soc.* **2022**, *47*, 3083–3090, (In Chinese with abstract in English). [[CrossRef](#)]
42. Ruan, Z.; Li, C.P.; Wu, A.X.; Wang, Y. A new risk assessment model for underground mine water inrush based on AHP and D-S evidence theory. *Mine Water Environ.* **2019**, *38*, 488–496. [[CrossRef](#)]
43. Saaty, T.L. A scaling method for priorities in hierarchical structures. *J. Math. Psychol.* **1977**, *15*, 234–281. [[CrossRef](#)]
44. Dong, S.N.; Zhou, W.F.; Wang, H. Introduction to special issue on mine water inrushes: Risk assessment, mitigation, and prevention. *Mine Water Environ.* **2021**, *40*, 321–333. [[CrossRef](#)]

Disclaimer/Publisher’s Note: The statements, opinions and data contained in all publications are solely those of the individual author(s) and contributor(s) and not of MDPI and/or the editor(s). MDPI and/or the editor(s) disclaim responsibility for any injury to people or property resulting from any ideas, methods, instructions or products referred to in the content.